



**ARTICLE**

# Influences of Multi-Component Supplementary Cementitious Materials on the Performance of Metakaolin Based Geopolymer

Wu Jing<sup>1,2,#</sup>, Ren Luo<sup>3,#</sup>, Sha Ding<sup>2</sup> and Ping Duan<sup>3,4,5,6,7,\*</sup>

<sup>1</sup>School of Civil Engineering and Architecture, Wuhan University of Technology, Wuhan, 430070, China

<sup>2</sup>Wuhan Hanyang Municipal Construction Group Co., Ltd., Wuhan, 430050, China

<sup>3</sup>Faculty of Materials Science and Chemistry, Key Laboratory of Geological Survey and Evaluation of Ministry of Education, China University of Geosciences, Wuhan, 430074, China

<sup>4</sup>Guangxi Key Laboratory of New Energy and Building Energy Saving, Guilin University of Technology, Guilin, 541004, China

<sup>5</sup>Zhejiang Institute, China University of Geosciences (Wuhan), Hangzhou, 311305, China

<sup>6</sup>Key Laboratory of Advanced Building Materials of Anhui Province, Anhui Jianzhu University, Hefei, 230022, China

<sup>7</sup>Key Laboratory of Road Structure and Materials of Ministry of Transport, Chang'an University, Xi'an, 710064, China

\*Corresponding Author: Ping Duan. Email: duanping@cug.edu.cn

#These authors contributed equally to this work

Received: 16 August 2021 Accepted: 14 October 2021

## ABSTRACT

In this study, the workability and reaction mechanism of metakaolin (MK) based geopolymer blended with rice husk ash (RHA) and silica fume (SF) was investigated. The prepared samples were subjected to tests including compressive strength and fluidity tests. X-ray diffraction (XRD) and Scanning electron microscope (SEM) were employed to explore the phase composition and microstructure of geopolymers. The molecular bonding information of geopolymer was provided by Fourier transform infrared spectroscopy (FTIR). Meanwhile, the porosity of geopolymer was obtained by Mercury intrusion porosimeter (MIP) analysis. The high-activity RHA obtained after calcination at 600°C was used as a supplementary cementitious material to prepare geopolymer. The properties of preventing morphology cracking and compressive strength are improved. The addition of RHA and SF changes the working performance of MK based geopolymer and provided a theoretical basis for future practical applications. Meanwhile, the high chemical activity of SF and RHA contributes to the healing of microcracks.

## KEYWORDS

Rice husk ash; silica fume; metakaolin; geopolymer

## 1 Introduction

Every 1 ton of Portland cement produced will emit about 0.8 tons of CO<sub>2</sub> emissions [1,2]. The annual CO<sub>2</sub> emissions from cement production are about 1.5 billion tons, which is about 6% of the total global greenhouse gas emissions [3]. The calcined production of traditional cement has brought severe environmental pressure to the world. Compared with traditional cement-based gels, geopolymers are a kind of low-carbon gels co-prepared by using multi-source aluminosilicate solid wastes, and have become a hot issue topic at home and abroad. Geopolymer is not only an important way to recycle bulk industrial



solid waste to develop green building materials, but also can meet the urgent needs of sustainable development in the building materials industry. Solid waste recycling has a profound impact on the construction of ecological civilization and the supply of resources [4]. Researchers working on green building materials have proposed the use of industrial solid waste materials to chemically stimulate the preparation of geopolymers as an effective alternative material.

Rice husks are the main by-product of rice. The surface of the rice husk is hard, high  $\text{SiO}_2$  content, which is not easy to be decomposed by bacteria. In recent years, many grain processing enterprises and power companies have started to use rice husk as biomass fuel for chemical production or power generation and heating. RHA accounts for about 20% of the weight of rice husks. RHA has the characteristics of large volume and small specific gravity. If RHA is not recycled in time, it will cause re-pollution to the environment. Therefore, the large-scale and high-value utilization of RHA is worthy of further study. The main components of RHA are carbon and  $\text{SiO}_2$ . With the change of combustion conditions, the silicon and remaining carbon content in RHA also change.

The  $\text{SiO}_2$  in RHA remains amorphous after low-temperature combustion and has a nanostructure [5]. Many studies [6–8] have shown that the specific surface of RHA is very large, so RHA is considered to be a porous pozzolanic material.

It is of great significance to realize the exploitation and utilization of rice husks as solid waste materials in the industry. Buyondo et al. [9] used RHA, MK and alkaline activators to prepare geopolymers and optimized production parameters using response surface methodology. Zhang et al. [10] used RHA to replace FA in high strength cement-based composites. The consequences show that the replacement of FA with RHA accelerates the pozzolanic reaction and improves the pore distribution in the ECC matrix. Zhu et al. [11] used isothermal calorimetry to explore the kinetic mechanism of RHA to MK based geopolymers. The effect of RHA content on the pore development and thermal stability of MK based geopolymer was further investigated. Billong et al. [8] explored the impact of NaOH solution as the activator and RHA content on microstructure of MK based geopolymer paste. The addition of RHA can improve the workability of the geopolymer. Shturm et al. [12] prepared RHA geopolymers using sodium aluminate solution as an activator. The effects of sodium aluminate on the microstructure of RHA geopolymer were researched. Kaur et al. [13] pointed out that RHA can be used as a gel, and then try to use different ratios of alkaline activator to find out the trend of its influence on properties of the geopolymer. Sharma et al. [14] show that RHA is effective in improving the hydration process of cement-based materials.

As a high-silicon active material, SF is often used in concrete modification. Chen et al. [15] found that filling cement void with MK and SF makes the structure of the gel denser. And in-depth consideration of the influence of the ratio of raw materials on the fluidity and hardening properties of the geopolymer paste. Kuzielová et al. [16] tried to use slag, SF, and MK instead of cement to prepare quaternary geopolymer. And compare the change of the internal voids in each group of samples. Meddah et al. [17] used MK and SF as partial substitutes for cement to prepare concrete. The results show that MK/SF mixed cement material has excellent resistance to chloride-ion erosion and freeze-thaw resistance. Alharbi et al. [18] tried to use SF to enhance reactive powder concrete, but the results obtained by mercury intrusion porosity test and compressive strength test methods showed that nanomaterials could not significantly enhance the mechanical characteristics of RPC .

Geopolymer has the advantages of early hardening and corrosion resistance, but defects such as high brittleness inhibit the application of geopolymer materials. The modification effect of geopolymer materials can be realized by adding specific modified fillers to the raw materials of geopolymer [19,20]. Nano-material activation and fiber-reinforced geopolymers are currently the main modification methods of geopolymer. Aygörmez et al. [21] prepared geopolymer by mixing SF, SL, Colemanite waste and MK,

and explored the resistance of geopolymer to acid solution erosion through micro-CT and other tests. Sahin's [22] study showed that PVA fiber could improve the mechanical properties of recycled aggregate geopolymer mortar, and explored its stability under high temperature and freeze-thaw cycles. Chu et al. [23] investigated the effect of carbon fiber on the processing properties of geopolymers from the perspective of fiber factors.

In order to accelerate the recycling process of RHA solid waste, rice husk calcined RHA and SF, two kinds of high silicon materials, were used to modify MK based geopolymer. The effects of RHA and SF on MK based geopolymers were studied, respectively, and the comprehensive effects of the two high silicon materials were further discussed. In order to explain the modification mechanism of MK based geopolymer by RHA and SF, we used SEM, XRD, FT-IR and other testing techniques to test different formulations of geopolymer samples. The action mechanism of RHA and SF in MK based geopolymer was further explored from two aspects of phenomenon and mechanism.

## 2 Materials and Methods

### 2.1 Materials

The MK used in the work was provided by Yunnan Tianhong Gaoling Mining Co., Ltd., China. The SF used in this work was obtained from Baotou, Inner Mongolia. The rice husks used in this work were provided by Jingzhou Agriculture Department in Hubei Province and were clean. The pericarp is shell-like and contains a lot of cellulose and lignin. In our previous study, it was found that high activity RHA could be obtained by calcination at 600°C. The alkali activator used in this work is water glass with an original modulus of 3.2 (Na<sub>2</sub>O 9.27 wt. %, SiO<sub>2</sub> 28.73 wt. %). NaOH (analysis reagent purity) was added into the alkali activator, and an alkaline silicate activator with a modulus of 1.5 (SiO<sub>2</sub>/Na<sub>2</sub>O molar ratio) was prepared. Then the activator was left standing at room temperature for 24 h. In order to better understand the physical properties of the raw materials on the formation of the polymerization system, materials used in this work were comprehensively characterized. The chemical composition of the solids was determined by X-ray fluorescence (XRF) and the results listed in Table 1.

**Table 1:** Chemical compositions of RHA, MK and SF provided by XRF analysis (wt. %)

	SiO <sub>2</sub>	Al <sub>2</sub> O <sub>3</sub>	Fe <sub>2</sub> O <sub>3</sub>	MgO	K <sub>2</sub> O	Na <sub>2</sub> O	CaO	P <sub>2</sub> O <sub>5</sub>	LOI
RHA	93.01	0.21	0.22	0.43	2.12	0.24	1.43	1.32	0.83
MK	53.33	43.35	1.69	0.22	0.39	0.17	0.02	0.05	0.86
SF	93.08	0.23	0.06	0.36	1.11	0.36	0.31	0.12	4.33

The particle size distribution parameter (D<sub>50</sub>) of MK, SF and RHA are 5.441, 18.31 and 25.73 μm. The results are shown in Fig. 1.

The crystal phases of MK, RHA and SF are shown in Fig. 2. MK is an anhydrous silicate aluminate clay obtained by calcination and dehydration of kaolin at 800°C. The lamellar structure of calcined kaolin is destroyed due to dehydration, so the crystallinity of MK is poor. As can be seen from Fig. 2, most of MK is amorphous silica-alumina material. In addition, impurities such as quartz, Muscovite and incompletely calcined kaolinite also exist in MK. Fig. 3a shows the SEM image of MK, and it can be found that the MK particles are irregular granular and lamellar structures with uneven size. XRD patterns of RHA and SF are shown in Fig. 2. As can be seen from the patterns, in the range of 2θ = 18~26°, there is a wide amorphous peak in the memory, which is the characteristic peak of amorphous SiO<sub>2</sub>, indicating the existence of amorphous silicon. Combined with the SiO<sub>2</sub> content of XRF and XRF, both RHA and SF have high content of amorphous silica, so the RHA and SF used in this study have high activity.

The microscopic morphology of SF is shown in Fig. 3b. It can be seen that SF is spherical, the diameter of spherical particles is less than 1  $\mu\text{m}$ , most of which are about 200 nm.

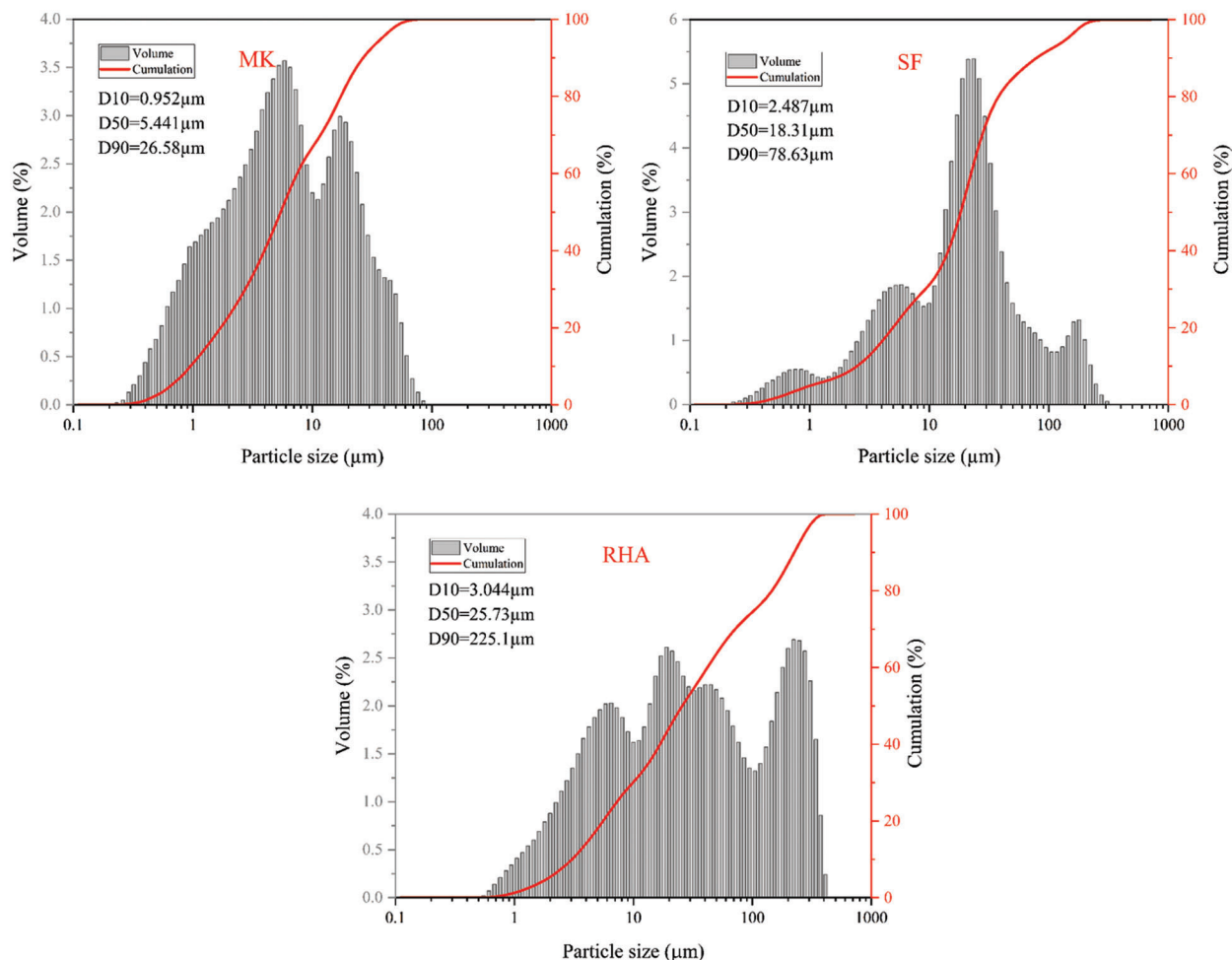


**Figure 1:** Size distribution of MK, SF and RHA

As can be seen from Fig. 4a, the original plant skeleton can be clearly seen in the high-temperature calcined rice husk at the magnification of 100  $\mu\text{m}$ , with relatively uniform and continuous bumps on the surface. At a magnification of 50  $\mu\text{m}$ , the flank of the RHA can clearly be seen as a sandwich structure consisting of intersecting and transversely superposed halves (Fig. 4b). The whole is loose, and there are many holes, a loose honeycomb shape. These holes are about 10  $\mu\text{m}$  in size, so they are easy to be detected by scanning electron microscopy. Further enlarging the RHA sample to 1  $\mu\text{m}$ , the lamina and lamina inside the RHA are composed of many fine  $\text{SiO}_2$  particles (Fig. 4c). Because the particle size is within the scale range of nanomaterials (0.1~100 nm), it is called nanogel particles (about 50 nm).

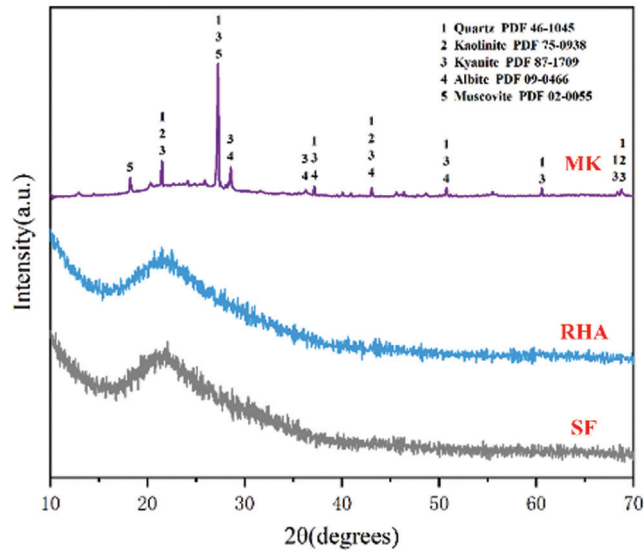


**Figure 2:** XRD patterns of MK, RHA and SF

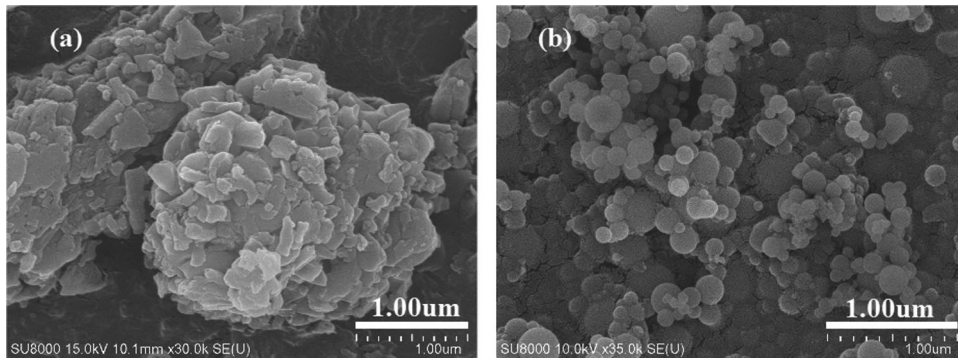


**Figure 3:** SEM image of MK (a) and SF (b)

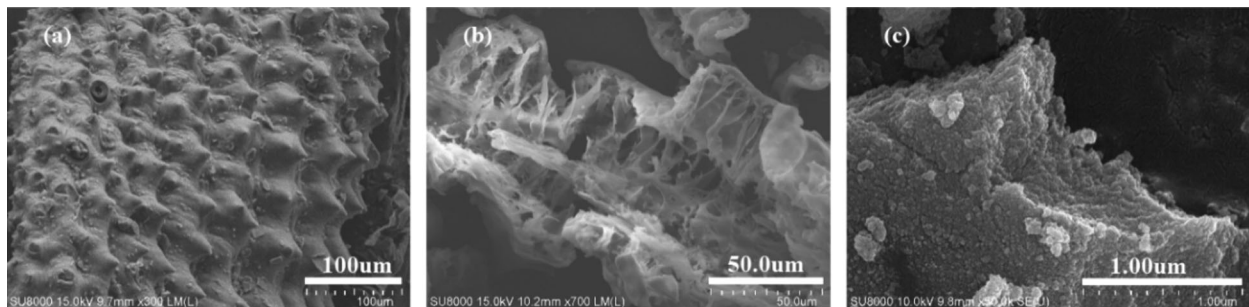


**Figure 4:** SEM image of RHA

## 2.2 Characterization

According to the fluidity test method of the national standard (GB/T 8077-2012), the fluidity of the mixed geopolymer paste was measured. According to the method in the national standard (GB/T 1346-2011), the setting time of the mixed geopolymer slurry was tested. The mechanical properties of

geopolymer were evaluated by using the CMT4202 electronic universal testing machine running at a rate of 5 kN/min.

The particle size distribution parameter ( $D_{50}$ ) of raw material was provided by a laser diffraction particle size analyzer (Masterizer 3000). The composition of the geopolymer was analyzed by X-ray diffractometer (X'Pert PRO MPD). The test conditions were as follows: Cu target  $K\alpha$  ray, the scanning step was  $0.02^\circ$ , and the scanning speed was 0.01 s/step. FTIR spectra of geopolymer were obtained with the Nicolet IS10 Fourier transform infrared spectrometer. Field emission scanning electron microscope (Hitachi SU8010) was used to analyze the microscopic morphology and composition of the sample.

The porosity and pore size percentage of the geopolymer were obtained by MIP. MICROMERITICS Auto-Pore 9200 V2.03 was used for the test, where the mercury contact Angle  $\theta$  was  $117^\circ$ .

### 2.3 Preparation of Geopolymer Paste

The composition of geopolymer paste is shown in Table 1, and sample preparation is shown in Fig. 5. First, pour MK, RHA and SF into the blender in turn according to the proportion in Table 2, and mix well. Then add the alkaline activator to the mixture in proportion and stir well. Under the condition that the mass ratio of activator to powder 0.8, geopolymer paste was prepared by alkali activation with different RHA, SF and MK. The prepared geopolymer slurry was poured into a  $40 \times 40 \times 40$  mm cubic mold. All samples were cured at room temperature for 24 h. All samples were removed from the mold and put into the standard constant temperature and humidity curing box for 3, 7 and 28 days under the standard curing conditions (humidity =  $95\% \pm 2\%$ , temperature:  $25^\circ\text{C} \pm 3^\circ\text{C}$ ).

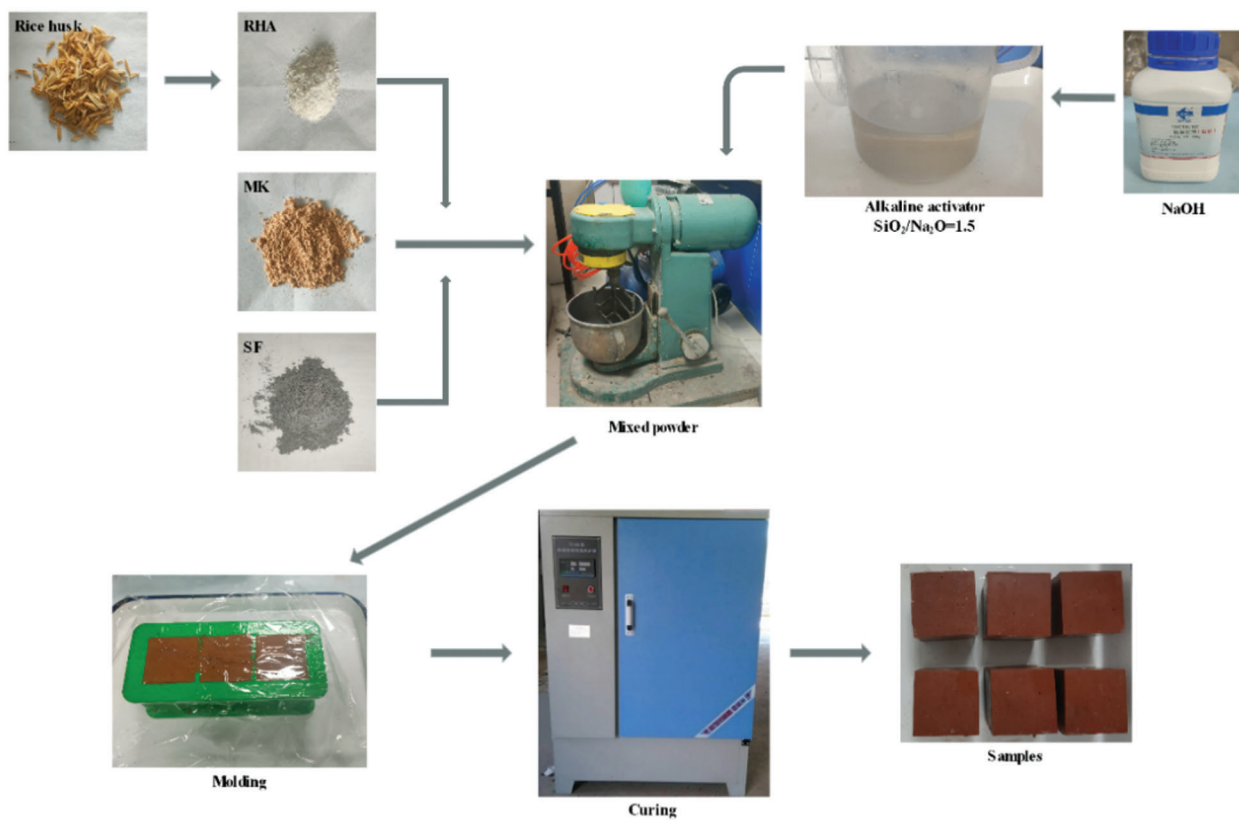


**Figure 5:** Flowchart of preparation of geopolymer

**Table 2:** Mix proportions of RHA-SF composite geopolymer

Samples	MK (kg/m <sup>3</sup> )	RHA (kg/m <sup>3</sup> )	SF (kg/m <sup>3</sup> )	Activator (kg/m <sup>3</sup> )
No. 1	1173.6	0	0	939
No. 2	1058.1	55.7	0	891
No. 3	959.6	106.6	0	853
No. 4	883.6	155.9	0	831.6
No. 5	818	204.5	0	818
No. 6	1107.2	0	58.3	932.4
No. 7	1044.1	0	116	928.1
No. 8	981.5	0	173.2	923.8
No. 9	911.2	0	227.8	911.2
No. 10	1013.5	56.3	56.3	900.9
No. 11	932	54.8	109.7	877.2
No. 12	910	107.1	53.5	856.5
No. 13	845.7	105.7	105.7	845.7

### 3 Results and Discussion

#### 3.1 Fluidity of Geopolymer Paste

The solidification of geopolymer is due to a certain amount of three-dimensional network structure generated by condensation polymerization inside the geopolymer matrix, which is reflected as the strength change macroscopically. The reaction rate and strength of geopolymers are essential prerequisites for their practical application [24]. The fluidity of composite geopolymer paste with different mix ratios is shown in Fig. 6. It can be observed that compared with Group No. 1, the fluidity of geopolymer pastes in Group No. 2 to No. 5 reduces. The experimental consequences show that the fluidity of composite geopolymer paste decreases with the increasing RHA content. After RHA partially replaces the content of MK, the volume added to RHA will be greater than that of MK [25]. In addition, RHA is a honeycomb structure composed of nanogel particles, and there are a lot of gaps between nanogel particles. A large number of pores in RHA absorb water in the composite gel system, resulting in the decreasing fluidity.

As can be seen from the figure, compared with Group No. 1, the fluidity of geopolymer paste in Group No. 6 to No. 9 gradually increases. The experimental results show that the fluidity of composite geopolymer paste increases with the increasing SF content. Since SF is a small spherical particle, it has a ball effect. Moreover, due to the size effect, the spherical silica particles are closely distributed in the MK void, which increases the fluidity of the geopolymer paste [26].

The results show that the fluidity of geopolymer paste in Group No. 10 is better than that of Group No. 12. The fluidity of geopolymer paste in Group No. 11 is better than that of Group No. 13. This phenomenon further proves the negative influence of RHA on the fluidity of composite geopolymer paste. Moreover, the fluidity of geopolymer pastes in Group No. 10 to No. 13 are not much different from that of the blank sample, which is the result of the interaction between the honeycomb structure of RHA and the structure of SF microspheres.

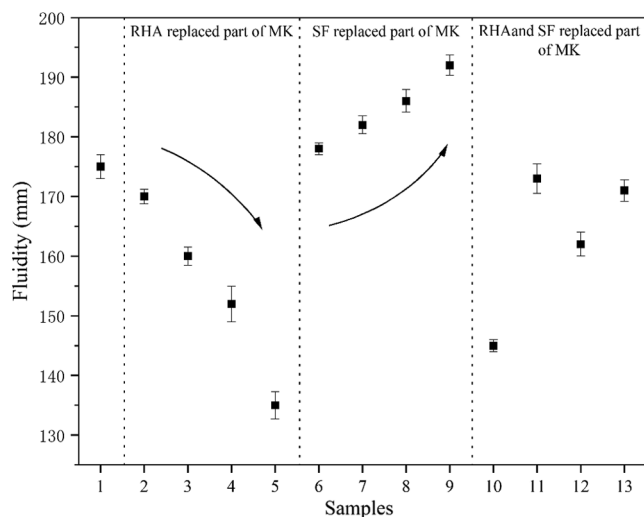


**Figure 6:** Fluidity of geopolymers

### 3.2 Determine the Setting Time of Geopolymer Paste

Fig. 7 shows the influence trend of RHA content on the setting time of MK based geopolymer. It can be seen from the test results that compared with Group No. 1, the initial and final setting time of Group No. 2 to No. 5 binary geopolymers are gradually shortened. Two main factors lead to the shortening of the condensation time. On the one hand, the porous structure of RHA can absorb water quickly, thus promoting the progress of geopolymerization. On the other hand, RHA with high activity reacts faster with alkaline activator, thus reducing the setting time.

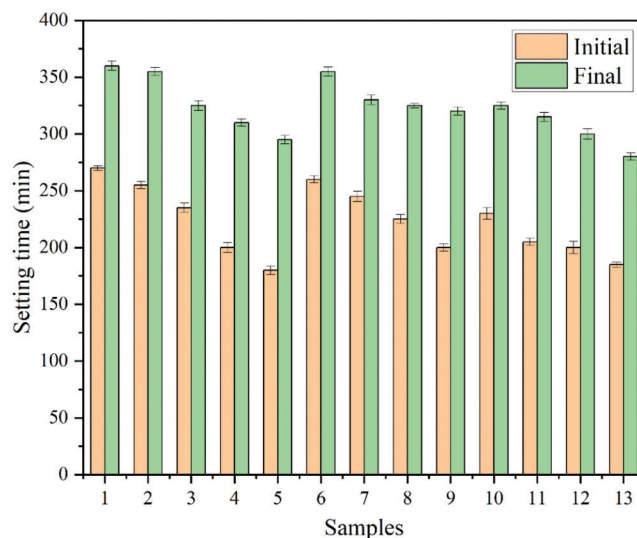


**Figure 7:** Setting time of geopolymers

Compared with Group No. 1, the initial and final condensation time of geopolymer in Group No. 5 (RHA instead of 20% MK) are shortened by 90 and 65 min, respectively. This is similar to the findings of Mejia et al. [27]. Compared with Group No. 1, the initial and final condensation time of Group No. 6 to No. 9 binary geopolymers are reduced. The results show that with the increasing SF content, the

setting time of MK based geopolymer decrease. SF with high reactivity accelerates the geopolymerization reaction, which leads to the shortening of the setting time [28]. Compared with Group No. 1, the initial and final condensation time of geopolymer in Group No. 9 (SF instead of 20% MK) are shortened by 70 and 40 min, respectively. This indicates that SF has a rapid coagulation effect.

It can be seen from the test results that compared with Group No. 1, the initial and final condensation time of Group No. 10 to No. 13 ternary geopolymers are gradually shortened. This is the result of the interaction between RHA and SF. The initial and final condensation time of geopolymer in Group No. 13 (RHA instead of 10% MK, SF instead of 10% MK) are reduced by 85 and 80 min, respectively.

### 3.3 Compressive Strength Analysis of Geopolymer

Fig. 8 shows the compressive strengths of geopolymer with different contents of RHA or SF at 3, 7 and 28 days of curing. As the curing age increases, the compressive strength of all samples increases significantly, which is attributed to the densification of structure and the deepening of geopolymerization degree. The Fig. 8 shows that with a certain range, the compressive strength of RHA-MK binary geopolymer gradually increases as the increasing of RHA content. RHA improves the compressive strength, which is due to the fact that part of the RHA participates in the geopolymerization as a silicon source and the unreacted RHA fills the voids of the geopolymer. The porous structure of RHA leads to water storage in the geopolymer in the early stage of reaction. When the water in the system is insufficient for geopolymerization, the water in the RHA migrates outward. Thus the internal curing environment is formed to allow the geopolymerization to continue [29]. The effect of RHA on the refinement of the pore structure and internal curing improves the compressive strength, which is similar to the consequences obtained by Yang et al. [30]. When the RHA content is 15% (Group No. 4), the compressive strength of RHA-MK binary geopolymer reached the peak values at 3, 7 and 28 days.

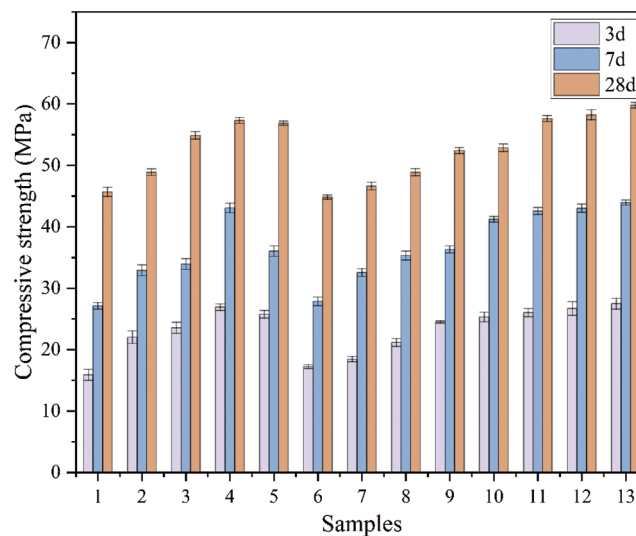


**Figure 8:** Compression strength of RHA-SF composite geopolymers

The compressive strength of the geopolymer increased from 15.89 to 26.91 MPa at three days of curing (RHA replaced 15% of MK), and increased from 27.13 to 43.07 MPa at seven days (RHA replaced 15% of MK). After curing for twenty-eight days, the binary geopolymer increased from 45.68 to 57.30 MPa (RHA replaced 15% of MK). However, When the RHA content exceeds 15%, the compressive strength of RHA-MK binary geopolymer decreases, which is caused by the creation of interlocking pores in the geopolymer

gel system due to excessive RHA [5]. Compared with Group No. 1, the compressive strength of SF-MK binary geopolymer gradually increases as the increasing SF content. Because SF replaces part of the MK content, high-activity  $\text{SiO}_2$  with larger specific surface area can be obtained to participate in geopolymerization [31]. At the same time, the SF particles are evenly distributed in the geopolymer matrix, and the denser three-dimensional structure is obtained through alkali-activated, which is also proved by Sheikhhosseini et al. [32].

When the SF content is 20% (Group No. 9), the compressive strength of the SF-MK binary geopolymer reaches the peak value after curing for 3, 7 and 28 days. Compared with Group No. 1, the compressive strength of the geopolymer increased from 15.89 to 24.47 MPa at three days of curing (SF replaced 20% of MK), and increased from 27.13 to 38.31 MPa at seven days (SF replaced 20% of MK). After curing for twenty-eight days, the binary geopolymer increased from 45.68 to 52.41 MPa (SF replaced 20% of MK).

Both RHA and SF can improve properties of composite geopolymer. The porous structure of RHA and the spherical structure of SF act different role in geopolymer matrix. Fig. 8 shows the compressive strength data of Group No. 10 to No. 13 ternary geopolymers. The results show that, compared with Group No. 1, the compressive strengths of Group No. 10 to No. 13 geopolymers at 3, 7 and 28 days are all significantly improved. This can be attributed to the void filling effect of SF particles and the internal curing effect of RHA. Further analysis shows that SF particles are smaller than RHA and fill the void of RHA fibers. However, amorphous  $\text{SiO}_2$  particles are enriched on the surface of RHA after calcination. Geopolymerization process occurred under the action of alkaline activator. Compared with Group No. 1, the compressive strength of Group No. 13 geopolymer (SF and RHA replaced 10% MK respectively) increased by 11.59, 16.81 and 14.10 MPa, respectively, after curing for 3, 7 and 28 days. Compared with the compressive strength consequences of Group No. 4, Group No. 9 and Group No. 13 geopolymers, it demonstrates that the strength of MK based geopolymer with compounding RHA and SF is better than that of single compounding.

### 3.4 X-Ray Diffraction Analysis of Geopolymer

XRD tests were performed on four groups of samples to explore the phase composition of geopolymers further. After 28 days of curing under standard curing conditions, the XRD patterns of geopolymers in Group No. 1, Group No. 4, Group No. 9 and Group No. 13 are shown in Fig. 9. The interior of the geopolymer gel is a three-dimensional network structure ranging from amorphous to semi-crystalline. The broad peak at  $2\theta = 18\text{--}36^\circ$  is its characteristic amorphous peak. The material corresponding to the characteristic peak Q in Fig. 9 belongs to the crystal phase, which is the unreacted component from the raw material [33]. The XRD analysis consequences show that the addition of RHA and SF has little effect on the crystal phase composition and structure of geopolymer. No new crystal phase is formed in the geopolymerization. At the same time, this also shows that RHA and SF form a relatively stable matrix in the MK based geopolymer.

### 3.5 FT-IR Analysis of Geopolymer

The FTIR spectra of the four geopolymer samples in Group No. 1, Group No. 4, Group No. 9 and Group No. 13 are shown in Fig. 10. It can be found that the absorption peak at about  $457\text{ cm}^{-1}$  is related to the in-plane bending vibration of the Si-O-Si bond in the  $[\text{SiO}_4]$  tetrahedron. The peak at band  $557\text{ cm}^{-1}$  is attributed to the symmetrical tensile vibration of the kaolinite Si-O-Al bond [34–36]. Due to the reorganization of  $[\text{TO}_4]$  (T stands for Al and Si) units in the formation of geopolymers, the asymmetric tensile vibration of T-O-Si bond is formed in the region of  $900\text{--}1,200\text{ cm}^{-1}$ . The wide vibration bands at  $1,050, 1,085, 1,083$  and  $1,048\text{ cm}^{-1}$  are the asymmetric stretching vibrations of the Si-O-T bond [37–40]. The vibrations around  $1,600$  and  $3,440\text{ cm}^{-1}$  are attributed to the vibrations of the hydroxyl in the water [41] contained in the sample (a-O-H in tension and H-O-H in bending). Under the same drying conditions, the vibrations of samples in Group No. 4 and Group No. 13 at the wave bands of about

1600 and 3440  $\text{cm}^{-1}$  were more prominent, indicating that the samples had better water absorption performance. This also indirectly proves that RHA has a better effect of adsorbing water and has an internal curing effect.

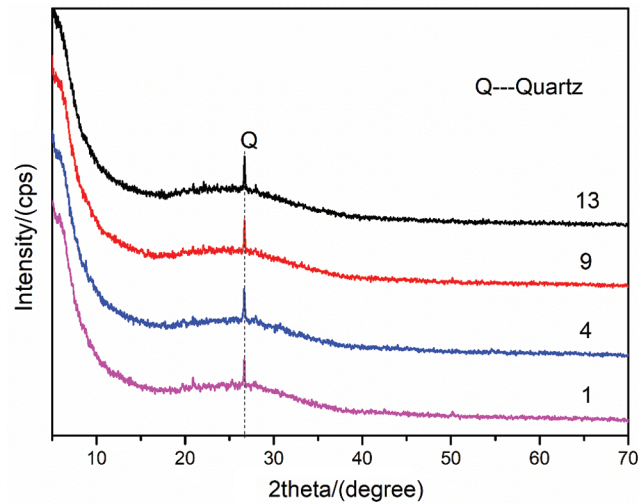


**Figure 9:** XRD patterns of geopolymers under standard curing for 28 days (No. 1: blank sample, No. 4: 15% RHA, No. 9: 20% SF and No. 13: 10% RHA and 10% SF)

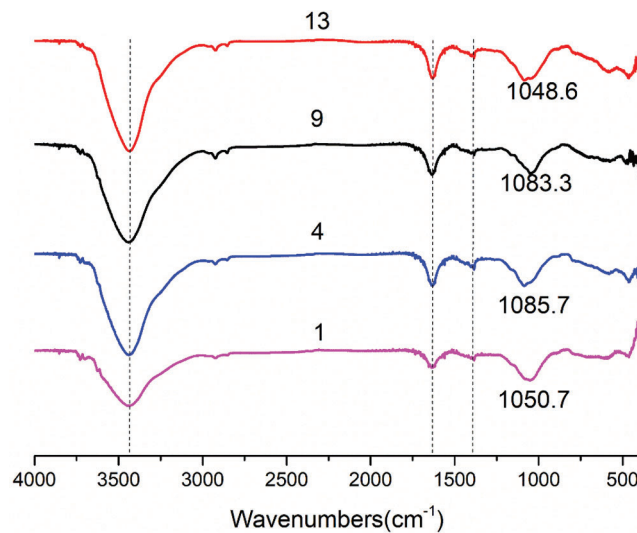


**Figure 10:** FT-IR spectrum of geopolymers under standard curing for 28 days (No. 1: blank sample, No. 4: 15% RHA, No. 9: 20% SF and No. 13: 10% RHA and 10% SF)

### 3.6 Microscopic Morphology of Geopolymer

SEM analysis is carried out on the four groups of geopolymer samples in Group No. 1, Group No. 4, Group No. 9 and Group No. 13. After 28 days of standard curing, the microstructures of the fractures of the four groups of geopolymer samples are shown in Fig. 11. Under the same microscope magnification, it can be found that there are more cracks on the surface of samples in Group No. 1 and relatively few cracks on the surface of geopolymer in Group No. 9. After adding RHA, the cracks of geopolymers in

Group No. 4 and Group No. 13 are more minor. The consequences show that the addition of RHA and SF can reduce the generation of microcracks, and the effect of RHA is better than that of SF. The inherent porous structure of RHA can store a certain amount of water and play an internal maintenance role to compensate for the adverse effects of the cracking of geopolymer [8]. By comparing Group No. 1 and Group No. 9, it can be found that the microstructure of geopolymer after adding SF is denser, which is the result of the space-filling influence of SF spherical particles. According to the characteristics of RHA and SF, the prepared terpolymer (in Group No. 13) has the least microcracks, dense structure and the best mechanical properties.

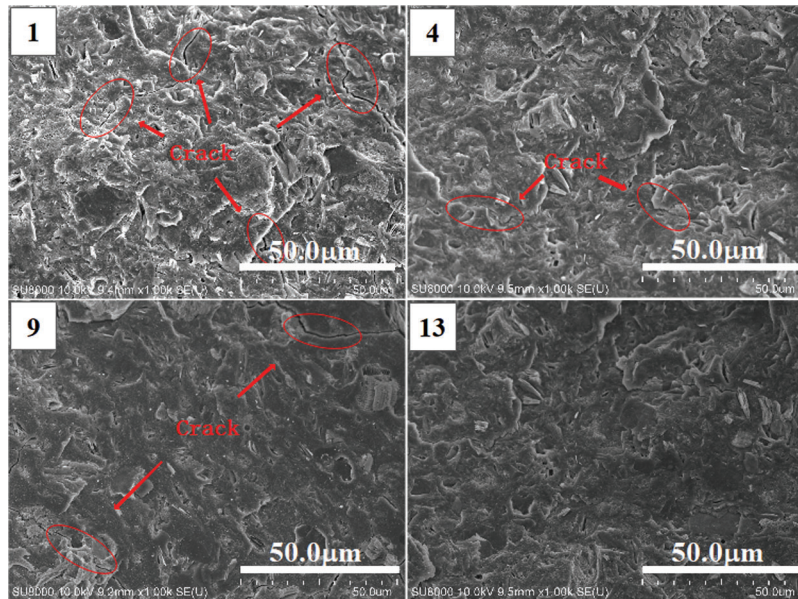


**Figure 11:** SEM image of broken surface of geopolymers under standard curing for 28 days (No. 1: blank sample, No. 4: 15% RHA, No. 9: 20% SF and No. 13: 10% RHA and 10% SF)

### 3.7 Porosity Analysis of Geopolymer

Changes in pore size percentage of geopolymers are provided by MIP. The outcomes are given in Figs. 12a and 12b. Fig. 12 shows the pore size percentage and porosity of the four geopolymer samples in Group No. 1, Group No. 4, Group No. 9 and Group No. 13 after 28 days of curing under standard curing conditions. It can be clearly shown from Fig. 12a that with the addition of RHA and SF, the cumulative pore volume of the corresponding sample gradually decreases. This indicates that the synergistic effect of RHA and SF can significantly refine the pore structure of the geopolymer. In addition, the spatial packing effect of SF spherical particles can make the structure of geopolymer denser. The incorporation of RHA and SF makes the microstructure of the geopolymer more compact, resulting in Group No. 13 showing a lower porosity. From the pore size percentage consequences shown in Fig. 12b, with the addition of RHA and SF, the change in total porosity is mainly attributed to the increase in the volume of the pores smaller than 10 nm and the decrease in the volume of the pores larger than  $10^4$  nm. The change of pore volume between 10 and  $10^4$  nm is relatively small. The volume of pores larger than  $10^4$  nm in Group No. 1 is obviously more than that in Group No. 4 and Group No. 9. Macroscopically, the compressive strength of Group No. 4 and Group No. 9 is obviously greater than that

of Group No. 1 sample. Compared with the other three groups, Group No. 13 has the least volume of pores larger than  $10^4$  nm, and the largest volume of pores less than 10 nm. Therefore, it can be proved that the optimal compressive strength of MK geopolymer can be obtained when prepared by SF and RHA composite incorporation is the best. By comparing MIP and compressive strength test results, it can be concluded that the smaller the cumulative pore volume is, and the less the compressive strength loss of geopolymer is [42,43].

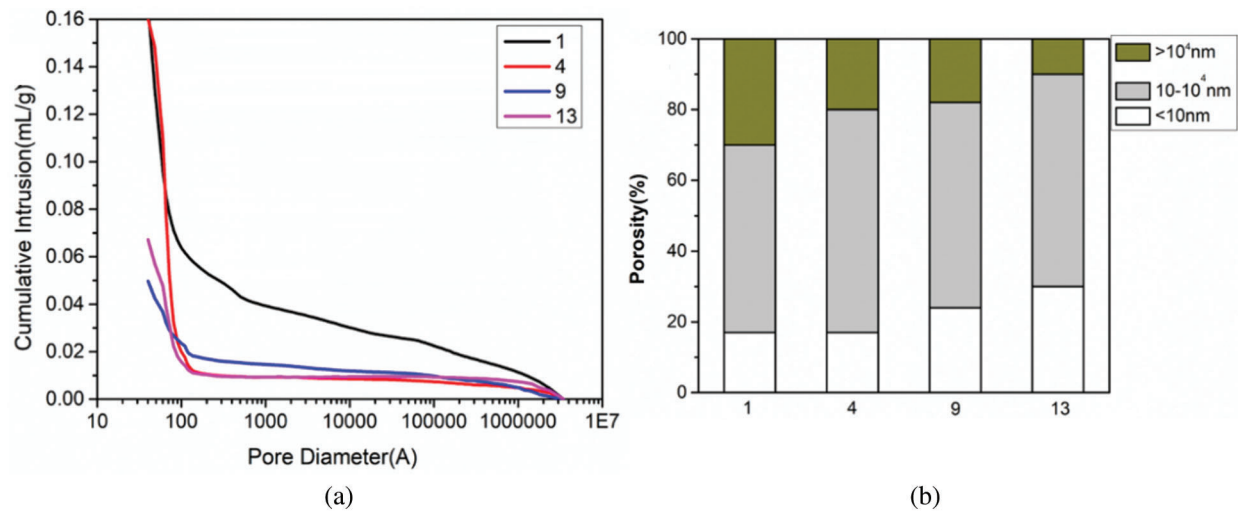


**Figure 12:** Porosity (a) and Pore size percentage (b) of geopolymers under standard curing for 28 days (No. 1: blank sample, No. 4: 15% RHA, No. 9: 20% SF and No. 13: 10% RHA and 10% SF)

#### 4 Conclusions

Based on analysis and result, the main conclusions are as follows:

1. With the increasing RHA content, the fluidity of RHA-MK binary geopolymer paste decreases, the initial and final setting time are shortened, and the compressive strength shows a trend of first increasing and then decreasing. With the increasing SF content, the fluidity of SF-MK binary geopolymer paste increased, and the initial and final setting time decreased. and the compressive strength of the geopolymer increases.

2. When RHA content is 15%, the compressive strength of geopolymer is the highest after curing for 28 days, which can reach 57.3 MPa. When the content of SF is 20%, the compressive strength of geopolymer is the highest after curing for 28 days, which can reach 52.41 MPa. When the content of RHA and SF are both 10%, the compressive strength of RHA-SF-MK ternary geopolymer reaches the maximum at 28 days, which can reach 60 MPa. The results show that the supplementary cementitious materials with RHA and SF have the best mechanical properties. Owing to the internal curing effect of RHA, the compressive strength of geopolymer can be improved by adding RHA.

3. The introduction of RHA and SF did not change the crystal phase of MK based geopolymer. The addition of RHA and SF makes the microstructure of the geopolymer more denser. The microcracks of the geopolymer containing RHA are significantly reduced.

4. Both RHA and SF can promote the progress of geopolymerization, improve the mechanical properties of geopolymer, and the enhancement effect of RHA is better. Because RHA has a honeycomb structure formed by highly active SiO<sub>2</sub> particles, the porous structure and internal curing effect improve the microscopic pore structure of the gel.

**Acknowledgement:** We thank the Faculty of Materials Science and Chemistry, Key Laboratory of Geological Survey and Evaluation of Ministry of Education, China University of Geosciences, Wuhan 430074, China for providing experimental conditions and funding for this research.

**Funding Statement:** The research presented in this paper was supported by Natural Science Foundation of Hubei Province (No. 2020CFB575), Natural Science Foundation of Zhejiang Province (No. LY19E080003), the Opening Fund of Key Laboratory of Geological Survey and Evaluation of Ministry of Education (Grant No. GLAB2020ZR09), the Fundamental Research Funds for the Central Universities, China University of Geosciences (Wuhan) and the Opening Fund of Guangxi Key Laboratory of New Energy and Building Energy Saving (Grant No. 19-J-22-2), Key Research and Development Program of Hubei Province (Grant No. 2020BAB065), Key Research and Development Program of Jiangxi Province (Grant No. 20201BBG71011), Fundamental Research Funds for the Central Universities, CHD (Grant No. 300102211506), Opening Fund of Key Laboratory of Advanced Building Materials of Anhui Province (Grant No. JZCL001KF).

**Conflicts of Interest:** The authors declare that they have no conflicts of interest to report regarding the present study.

## References

1. Scrivener, K. L., Kirkpatrick, R. J. (2008). Innovation in use and research on cementitious material. *Cement and Concrete Research*, 38(2), 128–136. DOI 10.1016/j.cemconres.2007.09.025.
2. Janssens-Maenhout, G., Crippa, M., Guizzardi, D., Muntean, M., Schaaf, E. et al. (2019). EDGAR v4.3.2 global atlas of the three major greenhouse gas emissions for the period 1970–2012. *Earth System Science Data*, 11(3), 959–1002. DOI 10.5194/essd-11-959-2019.
3. Amran, Y. H. M., Alyousef, R., Alabduljabbar, H., El-Zeadani, M. (2020). Clean production and properties of geopolymer concrete: A review. *Journal of Cleaner Production*, 251(SPE2), 119679. DOI 10.1016/j.jclepro.2019.119679.
4. Chu, S. H., Poon, C. S., Lam, C. S., Li, L. (2021). Effect of natural and recycled aggregate packing on properties of concrete blocks. *Construction and Building Materials*, 278(9), 122247. DOI 10.1016/j.conbuildmat.2021.122247.
5. Liu, X., Jiang, J., Zhang, H., Li, M., Wu, Y. et al. (2020). Thermal stability and microstructure of metakaolin-based geopolymer blended with rice husk ash. *Applied Clay Science*, 196, 105769. DOI 10.1016/j.clay.2020.105769.
6. Nuaklong, P., Jongvivatsakul, P., Pothisiri, T., Sata, V., Chindaprasirt, P. (2020). Influence of rice husk ash on mechanical properties and fire resistance of recycled aggregate high-calcium fly ash geopolymer concrete. *Journal of Cleaner Production*, 252(5), 119797. DOI 10.1016/j.jclepro.2019.119797.
7. Mehta, A., Siddique, R. (2018). Sustainable geopolymer concrete using ground granulated blast furnace slag and rice husk ash: Strength and permeability properties. *Journal of Cleaner Production*, 205(2), 49–57. DOI 10.1016/j.jclepro.2018.08.313.
8. Billong, N., Kinuthia, J., Oti, J., Melo, U. C. (2018). Performance of sodium silicate free geopolymers from metakaolin (MK) and rice husk ash (RHA): Effect on tensile strength and microstructure. *Construction and Building Materials*, 189(6), 307–313. DOI 10.1016/j.conbuildmat.2018.09.001.
9. Buyondo, K. A., Olupot, P. W., Kirabira, J. B., Yusuf, A. A. (2020). Optimization of production parameters for rice husk ash-based geopolymer cement using response surface methodology. *Case Studies in Construction Materials*, 13(1), e00461. DOI 10.1016/j.cscm.2020.e00461.
10. Zhang, Z., Yang, F., Liu, J. C., Wang, S. (2020). Eco-friendly high strength, high ductility engineered cementitious composites (ECC) with substitution of fly ash by rice husk ash. *Cement and Concrete Research*, 137(2), 106200. DOI 10.1016/j.cemconres.2020.106200.

11. Zhu, H., Liang, G., Zhang, Z., Wu, Q., Du, J. (2019). Partial replacement of metakaolin with thermally treated rice husk ash in metakaolin-based geopolymer. *Construction and Building Materials*, 221(3), 527–538. DOI 10.1016/j.conbuildmat.2019.06.112.
12. Sturm, P., Gluth, G. J. G., Brouwers, H. J. H., Kühne, H. C. (2016). Synthesizing one-part geopolymers from rice husk ash. *Construction and Building Materials*, 124(3), 961–966. DOI 10.1016/j.conbuildmat.2016.08.017.
13. Kaur, K., Singh, J., Kaur, M. (2018). Compressive strength of rice husk ash based geopolymer: The effect of alkaline activator. *Construction and Building Materials*, 169, 188–192. DOI 10.1016/j.conbuildmat.2018.02.200.
14. Sharma, D. K., Sharma, R. (2018). Influence of rice husk ash and rice tiller ash along with chromate reducing agents on strength and hydration properties of ordinary Portland cement. *Construction and Building Materials*, 169(326), 843–850. DOI 10.1016/j.conbuildmat.2018.03.044.
15. Chen, J. J., Ng, P. L., Chu, S. H., Guan, G. X., Kwan, A. K. H. (2020). Ternary blending with metakaolin and silica fume to improve packing density and performance of binder paste. *Construction and Building Materials*, 252(1), 119031. DOI 10.1016/j.conbuildmat.2020.119031.
16. Kuzielová, E., Žemlička, M., Bartoničková, E., Palou, M. T. (2017). The correlation between porosity and mechanical properties of multicomponent systems consisting of Portland cement-slag-silica fume-metakaolin. *Construction and Building Materials*, 135, 306–314. DOI 10.1016/j.conbuildmat.2016.12.105.
17. Meddah, M. S., Ismail, M. A., El-Gamal, S., Fitriani, H. (2018). Performances evaluation of binary concrete designed with silica fume and metakaolin. *Construction and Building Materials*, 166(2), 400–412. DOI 10.1016/j.conbuildmat.2018.01.138.
18. Alharbi, Y. R., Abadel, A. A., Mayhoub, O. A., Kohail, M. (2021). Effect of using available metakaoline and nano materials on the behavior of reactive powder concrete. *Construction and Building Materials*, 269(7), 121344. DOI 10.1016/j.conbuildmat.2020.121344.
19. He, P., Jia, D., Lin, T., Wang, M., Zhou, Y. (2010). Effects of high-temperature heat treatment on the mechanical properties of unidirectional carbon fiber reinforced geopolymer composites. *Ceramics International*, 36(4), 1447–1453. DOI 10.1016/j.ceramint.2010.02.012.
20. Bernal, S., De Gutierrez, R., Delvasto, S., Rodriguez, E. (2010). Performance of an alkali-activated slag concrete reinforced with steel fibers. *Construction and Building Materials*, 24(2), 208–214. DOI 10.1016/j.conbuildmat.2007.10.027.
21. Aygörmez, Y., Canpolat, O. (2021). Long-term sulfuric and hydrochloric acid resistance of silica fume and colemanite waste reinforced metakaolin-based geopolymers. *Revista de la Construcción*, 20(2), 291–307. DOI 10.7764/RDLC.20.2.291.
22. Sahin, F., Uysal, M., Canpolat, O., Cosgun, T., Dehghanpour, H. (2021). The effect of polyvinyl fibers on metakaolin-based geopolymer mortars with different aggregate filling. *Construction and Building Materials*, 300(1), 124257. DOI 10.1016/j.conbuildmat.2021.124257.
23. Chu, S. H., Ye, H., Huang, L., Li, L. G. (2021). Carbon fiber reinforced geopolymer (FRG) mix design based on liquid film thickness. *Construction and Building Materials*, 269(9), 121278. DOI 10.1016/j.conbuildmat.2020.121278.
24. Yu, G. L., Jia, Y. M. (2021). Preparation of geopolymer composites based on alkali excitation. *Arabian Journal of Geosciences*, 14(7), 1–8. DOI 10.1007/s12517-021-06908-8.
25. Luo, Q., Wang, Y., Hong, S., Xing, F., Dong, B. (2021). Properties and microstructure of lithium-slag-based geopolymer by one-part mixing method. *Construction and Building Materials*, 273(5), 121723. DOI 10.1016/j.conbuildmat.2020.121723.
26. Ni, C., Wu, Q., Yu, Z., Shen, X. (2021). Hydration of Portland cement paste mixed with densified silica fume: From the point of view of fineness. *Construction and Building Materials*, 272(2), 121906. DOI 10.1016/j.conbuildmat.2020.121906.
27. Mejía, J. M., Mejía de Gutiérrez, R., Montes, C. (2016). Rice husk ash and spent diatomaceous earth as a source of silica to fabricate a geopolymeric binary binder. *Journal of Cleaner Production*, 118(5), 133–139. DOI 10.1016/j.jclepro.2016.01.057.

28. Kumar, M., Singh, S. K., Singh, N. P., Singh, N. B. (2012). Hydration of multicomponent composite cement: OPC-FA-SF-MK. *Construction and Building Materials*, 36(4), 681–686. DOI 10.1016/j.conbuildmat.2012.06.055.
29. Li, Z., Zhang, S., Liang, X., Granja, J., Azenha, M. et al. (2020). Internal curing of alkali-activated slag-fly ash paste with superabsorbent polymers. *Construction and Building Materials*, 263(2), 120985. DOI 10.1016/j.conbuildmat.2020.120985.
30. Yang, L., Shi, C., Wu, Z. (2019). Mitigation techniques for autogenous shrinkage of ultra-high-performance concrete—A review. *Composites Part B: Engineering*, 178(5), 107456. DOI 10.1016/j.compositesb.2019.107456.
31. Diaz, E. I., Allouche, E. N., Eklund, S. (2010). Factors affecting the suitability of fly ash as source material for geopolymers. *Fuel*, 89(5), 992–996. DOI 10.1016/j.fuel.2009.09.012.
32. Sheikhhosseini Lori, I., Toufigh, M. M., Toufigh, V. (2021). Improvement of poorly graded sandy soil by using copper mine tailing dam sediments-based geopolymer and silica fume. *Construction and Building Materials*, 281(2), 122591. DOI 10.1016/j.conbuildmat.2021.122591.
33. Çevik, A., Alzebaree, R., Humur, G., Niş, A., Gülşan, M. E. (2018). Effect of nano-silica on the chemical durability and mechanical performance of fly ash based geopolymer concrete. *Ceramics International*, 44(11), 12253–12264. DOI 10.1016/j.ceramint.2018.04.009.
34. Fernández-Jiménez, A., Palomo, A. (2005). Mid-infrared spectroscopic studies of alkali-activated fly ash structure. *Microporous and Mesoporous Materials*, 86(1), 207–214. DOI 10.1016/j.micromeso.2005.05.057.
35. Lee, W. K. W., van Deventer, J. S. J. (2002). Structural reorganisation of class F fly ash in alkaline silicate solutions. *Colloids and Surfaces A: Physicochemical and Engineering Aspects*, 211(1), 49–66. DOI 10.1016/S0927-7757(02)00237-6.
36. Okoye, F. N., Prakash, S., Singh, N. B. (2017). Durability of fly ash based geopolymer concrete in the presence of silica fume. *Journal of Cleaner Production*, 149(2), 1062–1067. DOI 10.1016/j.jclepro.2017.02.176.
37. Handke, M., Mozgawa, W. (1995). Model quasi-molecule Si<sub>2</sub>O as an approach in the IR spectra description glassy and crystalline framework silicates. *Journal of Molecular Structure*, 348, 341–344. DOI 10.1016/0022-2860(95)08658-I.
38. Zhang, Z., Wang, H., Provis, J. L., Bullen, F., Reid, A. et al. (2012). Quantitative kinetic and structural analysis of geopolymers. Part 1. The activation of metakaolin with sodium hydroxide. *Thermochimica Acta*, 539, 23–33. DOI 10.1016/j.tca.2012.03.021.
39. Vempati, R. K., Rao, A., Hess, T. R., Cocke, D. L., Lauer, H. V. (1994). Fractionation and characterization of texas lignite class 'F' fly ash by XRD, TGA, FTIR, and SFM. *Cement and Concrete Research*, 24(6), 1153–1164. DOI 10.1016/0008-8846(94)90039-6.
40. Chindaprasirt, P., Paisitsrisawat, P., Rattanasak, U. (2014). Strength and resistance to sulfate and sulfuric acid of ground fluidized bed combustion fly ash-silica fume alkali-activated composite. *Advanced Powder Technology*, 25(3), 1087–1093. DOI 10.1016/j.apt.2014.02.007.
41. Ma, X., Zhang, Z., Wang, A. (2016). The transition of fly ash-based geopolymer gels into ordered structures and the effect on the compressive strength. *Construction and Building Materials*, 104, 25–33. DOI 10.1016/j.conbuildmat.2015.12.049.
42. Guo, L., Wu, Y., Xu, F., Song, X., Ye, J. et al. (2020). Sulfate resistance of hybrid fiber reinforced metakaolin geopolymer composites. *Composites Part B: Engineering*, 183(450–451), 107689. DOI 10.1016/j.compositesb.2019.107689.
43. Ren, D., Yan, C., Duan, P., Zhang, Z., Li, L. et al. (2017). Durability performances of wollastonite, tremolite and basalt fiber-reinforced metakaolin geopolymer composites under sulfate and chloride attack. *Construction and Building Materials*, 134(5), 56–66. DOI 10.1016/j.conbuildmat.2016.12.103.